BBA - Molecular Cell Research 1867 (2020) 118726

Contents lists available at ScienceDirect

BBA - Molecular Cell Research

journal homepage: www.elsevier.com/locate/bbamcr

Apparent stiffness of vimentin intermediate filaments in living cells and its relation with other cytoskeletal polymers

Mariano Smoler[a], Giovanna Coceano[b], Ilaria Testa[b], Luciana Bruno[c], Valeria Levi[a,*]

[a] Universidad de Buenos Aires, Facultad de Ciencias Exactas y Naturales, Departamento de Química Biológica, Instituto de Química Biológica (IQUIBICEN), Ciudad de Buenos Aires, Argentina

[b] KTH Royal Institute of Technology, Department of Applied Physics and Science for Life Laboratory, 100 44, Stockholm, Sweden.

[c] Universidad de Buenos Aires, Facultad de Ciencias Exactas y Naturales, Instituto de Cálculo, Ciudad de Buenos Aires, Argentina.

ARTICLE INFO

Keywords:
Intermediate filaments
Single filament tracking
Live-cell microscopy
Persistence length
Cytoskeleton
Vimentin

ABSTRACT

The cytoskeleton is a complex network of interconnected biopolymers intimately involved in the generation and transmission of forces. Several mechanical properties of microtubules and actin filaments have been extensively explored in cells. In contrast, intermediate filaments (IFs) received comparatively less attention despite their central role in defining cell shape, motility and adhesion during physiological processes as well as in tumor progression. Here, we explored relevant biophysical properties of vimentin IFs in living cells combining confocal microscopy and a filament tracking routine that allows localizing filaments with ~20 nm precision. A Fourier-based analysis showed that IFs curvatures followed a thermal-like behavior characterized by an apparent persistence length (lp*) similar to that measured in aqueous solution. Additionally, we determined that certain perturbations of the cytoskeleton affect lp* and the lateral mobility of IFs as assessed in cells in which either the microtubule dynamic instability was reduced or actin filaments were partially depolymerized. Our results provide relevant clues on how vimentin IFs mechanically couple with microtubules and actin filaments in cells and support a role of this network in the response to mechanical stress.

1. Introduction

The ability of an eukaryotic cell to resist deformation, to transport organelles and vesicles and change its shape during processes such as cell migration depends on the cytoskeleton, a network of biopolymers formed by microtubules, actin filaments and intermediate filaments (IFs), in constant remodeling [1,2].

Internal and external physical forces act through the cytoskeleton and impact on many cell functions [3]. Thus, it is very relevant to understand how the network of cytoskeletal filaments is able to generate, transmit and respond to mechanical signals. Microtubules and actin filaments have been extensively explored due to their central role in processes such as cell division and intracellular transport; in contrast, IFs received comparatively less attention until recently.

Intermediate filaments contribute to the cell stiffness [4–6] and are involved in the organization of the cell cytoplasm [6–8]. Additionally, these filaments play central roles in processes such as cell migration [9–11], development [12], signal transduction and gene expression regulation [13]. In contrast to microtubules and actin filaments, the family of IFs filaments vary in their protein composition [14] and their relative abundance depends on the tissue, the cell type and its context [9].

In vitro studies with purified IFs revealed unique mechanical properties of IFs networks (reviewed in [15–17]). IFs are the softest component of the cytoskeleton; their persistence length (*i.e.*, the length of the filament over which thermal bending becomes appreciable [18]) ranges 0.2–3 μm depending on the IF composition and measurement conditions [19]. In contrast, the persistence lengths of actin and microtubules are ~15 μm and ~6 mm, respectively [18,20,21].

Vimentin filaments stand out as one of the most studied IFs due to their key role in cell migration [15,22]. Their expression increase during the epithelial to mesenchymal transition defining changes in cell shape, motility, and adhesion [4] required in physiological processes such as embryonic development as well as in tumor progression with metastatic expansion. Recently, it was demonstrated the vimentin IFs play a central role in protecting the cell nucleus during migration [23].

In vitro experiments showed that networks of these IFs withstand significantly greater mechanical deformation than actin and microtubules [24] with an elastic modulus that increases at large strains [25]. As other intracellular filaments, vimentin IFs are polyelectrolyte

* Corresponding author.
E-mail address: vlevi12@gmail.com (V. Levi).

https://doi.org/10.1016/j.bbamcr.2020.118726
Received 9 March 2020; Received in revised form 11 April 2020; Accepted 15 April 2020
Available online 19 April 2020
0167-4889/ © 2020 Elsevier B.V. All rights reserved.

polymers [26] that may crosslink in the presence of physiological concentrations of divalent cations such as Mg^{2+} or Ca^{2+}, and form bundles and other structures of increased rigidity [26,27].

In living cells, the different cytoskeletal filaments interact with each other through a wide variety of biomolecules including small protein crosslinkers, molecular motors and structures such as the plasma membrane or organelles [8,28–32]. Additionally, cytoskeletal filaments are not static structures but present continuous cycles of polymerization and depolymerization [18] giving the network another layer of complexity. Therefore, many properties of the cytoskeleton network cannot be explained by only considering the behavior of the filaments *in vitro*.

Here, we combine confocal imaging and a filament tracking procedure to explore certain biomechanical properties of vimentin IFs in living cells. Particularly, we analyze the lateral mobility and apparent persistence length of these filaments, properties that had provided relevant information on the mechanical behavior of other cytoskeletal filaments in their natural context [33,34]. We also study how perturbations introduced to the microtubule or actin filaments networks impact on IFs. This study provides information on how the vimentin IF network mechanically couples with other components of the cytoskeleton in live cells.

2. Materials and methods

2.1. Cell culture and transfection

Baby hamster kidney (BHK) cells were cultured in high glucose Dulbecco's Modified Eagle Medium (DMEM, Gibco) supplemented with 10% fetal bovine serum and 1% penicillin-streptomycin at 37 °C and 5% CO_2.

For microscopy measurements, cells were grown for 2 days on sterilized 25-mm coverslips and placed into 35-mm plates with 1.5 ml of complete medium.

Cells grown on coverslips were transfected using Lipofectamine 2000 (Invitrogen) with plasmids encoding GFP-vimentin, which co-assembles with endogenous vimentin [7] or EMTB-3xGFP [35], which codifies the microtubule-binding domain of ensconsin fused to a tandem of 3 copies of GFP (Addgene # 26741) and observed 24 h after transfection. These plasmids were kind gifts of Dr. V. I. Gelfand (Northwestern University, Chicago, IL) and Dr. Arpita Upadhyaya (University of Maryland, College Park, MD), respectively.

STED images were acquired in transformed and metastasizing BJ fibroblasts (BJF) constructed by Hahn et al. [36]. ~10^5 cells were grown for 24 h on 18-mm coverslips and then transiently transfected using Lipofectamine LTX Reagent with PLUS reagent (Thermo Fisher Scientific, #15338100), according to the manufacturer's instructions, with a plasmid coding for a EGFP-vimentin [37]. 24 h after transfection, cells were fixed (4% paraformaldehyde in PBS), permeabilized (Triton-X-100) and stained with a rabbit anti-GFP antibody (Abcam), and an Alexa488-conjugated secondary antibody (Abcam).

2.2. BHK cells treatments

Total and partial actin depolymerization were achieved by incubation of the cells with 0.15 or 1.5 μM latrunculin B for 30 min, respectively. Cells were incubated with 10 μM nocodazole during 30 min at 0 °C to depolymerize microtubules [38]; a similar treatment preserved vimentin IF organization in another cell line [39]. To reduce microtubule polymerization/depolymerization dynamics, cells were incubated with 30 nM vinblastine (Sigma-Aldrich) for 10 min [40]. The cell samples were observed within 30 min after these treatments.

To label the actin network, cells were fixed (4% paraformaldehyde in PBS), permeabilized with Triton X-100 (0.1% in PBS) and incubated with phalloidin-Texas Red X (Molecular Probes).

2.3. Confocal microscopy

Confocal images were acquired in a FV1000 confocal microscope (Olympus). GFP-tagged proteins were observed using a multi-line Ar laser tuned at 488 nm (0.3–1.5 μW at the sample) as excitation source. The laser light was reflected by a dichroic mirror and focused through a 60× oil immersion objective (NA = 1.35; Olympus, Japan) onto the sample. Fluorescence was collected by the same objective, passed through the pinhole, reflected on a diffraction grating and passed through a slit set to transmit in the range of 500–600 nm or 500–530 nm for one and two-color experiments, respectively.

Texas Red X-labeled actin filaments were observed using as excitation source a 543 nm diode laser (1 μW at the sample) and collecting the fluorescence in the range of 555–655 nm.

The fluorescence photons were detected with photomultipliers set in the photon-counting detection mode. The pixel size was set in the range of 65–100 nm.

For filament tracking experiments, we acquired image stacks of single cells during ~2 min with an acquisition speed of 0.3 frames/s.

2.4. Stimulated emission depletion (STED) microscopy

STED images were acquired on a TCS SP8 3× STED microscope (Leica) equipped with a 100×/1.4 STED WHITE objective. The images were recorded by exciting Alexa 488 with a 488 nm laser line and depleting with a STED beam at 592 nm. The pixel size was set to 20 nm.

2.5. Filament localization with nanometer accuracy

The coordinates of IFs segments were recovered from confocal images of GFP-vimentin transfected cells using the single-filament tracking routine AFTER [34]. Briefly, the program applies a rotation transformation to the image in such a way that the x_k coordinates of the filament are univocally associated to single y_k values. For each x_k, the algorithm extracts the intensity profile in the vertical direction and localizes the filament center with nanometer precision using a generalized regression neural network [41,42]. AFTER outperforms the traditional Gaussian deconvolution methods at the signal to noise ratios (S/N) observed in living cells thus providing the filament coordinates with smaller errors [34].

2.6. Fourier decomposition of filament shapes

We used the filament coordinates (x_k, y_k) recovered from the images to calculate tangent angles:

$$\theta_k = \tan^{-1}\left(\frac{y_{k+1} - y_k}{x_{k+1} - x_k}\right) \quad (1)$$

and segment lengths:

$$S_k = \sqrt{(x_{k+1} - x_k)^2 + (y_{k+1} - y_k)^2} \quad (2)$$

The tangent angle is then decomposed into a large number of Fourier modes and expressed as a sum of cosines [43]:

$$\theta(s) = \sqrt{2/L} \sum_{n=0}^{\infty} a_n \cos(q_n s) \quad (3)$$

where q_n represents the wave vector and is defined as $q_n = n\pi/L$. The zero-order term a_o corresponds to the average orientation of the filament, s is the arc length along the filament and L is the segment length.

2.7. Image analyses

Confocal images of cells labeled with Texas Red X-phalloidin (red channel) and expressing GFP-vimentin (green channel) were processed with specific FIJI tools [44]. The red channel images were binarized,

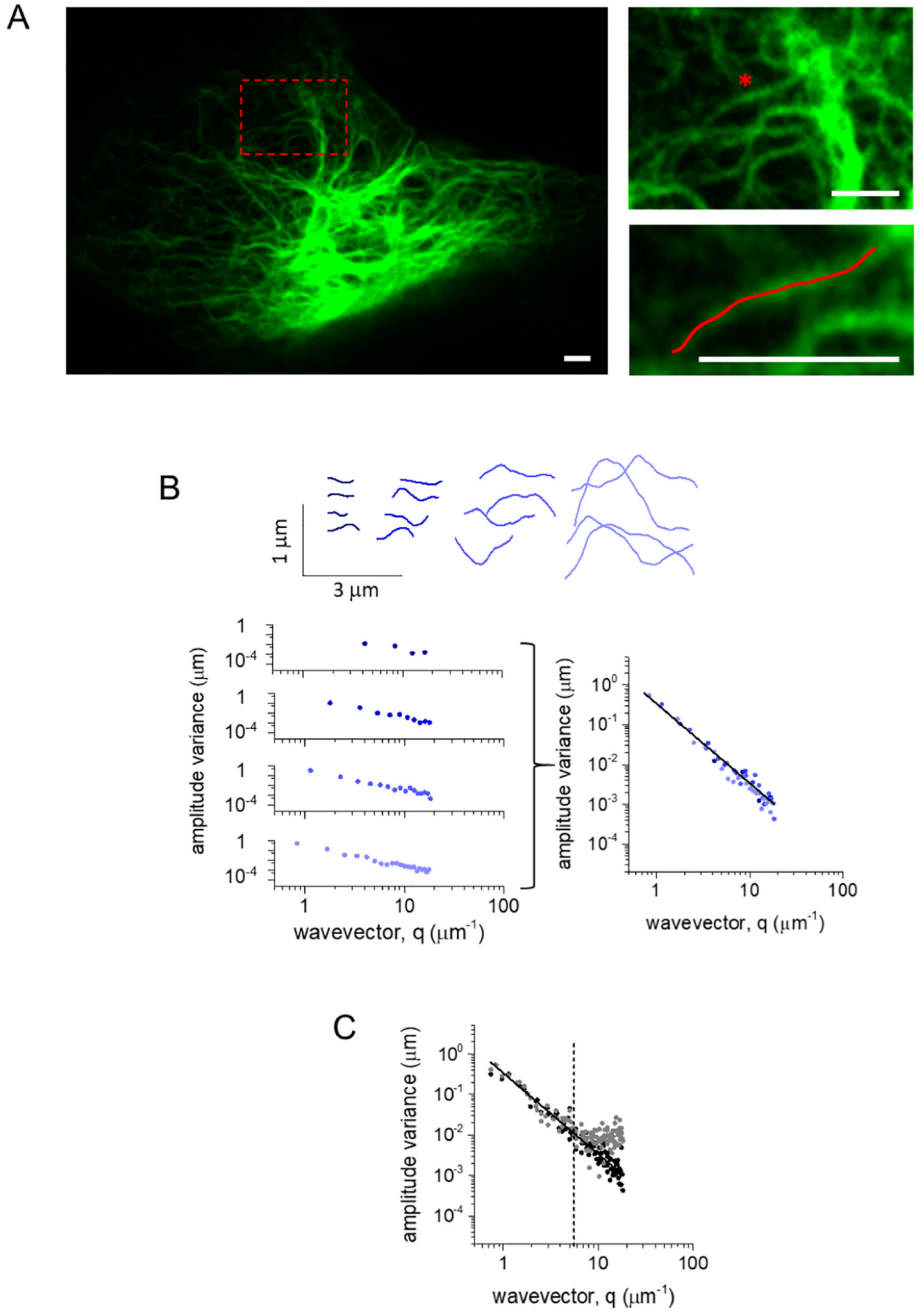

Fig. 1. Tracking vimentin filaments in living cells. (A) Representative confocal image of a BHK cell expressing GFP-vimentin. The right, top panel shows a zoom-in region of the cell (dotted rectangle in the left panel) with a filament (labeled with an asterisk) tracked using the AFTER routine (red line in bottom panel). Scale bars, 2 µm. To facilitate the visual observation, we used different intensity scales in the images. (B) Schematic representation of the Fourier analysis. The top panel shows simulated filaments with lp = 3 µm split into groups according to their relative lengths (colored in different blue tones). These shapes were Fourier-decomposed (central panel) and globally fit with Eq. (6) (continuous line). (C) Effects of the filament localization error in the Fourier analysis. The dotted line corresponds to the threshold mentioned in the text.

processed to eliminate open areas inside the mask perimeter and used to calculate the cell spreading area and the geometrical center of mass of the cell (CM_{cell}). The number of stress fibers in cells was estimated by eye inspection. The green channel images were despeckled and binarized to obtain the vimentin network area. The despeckled images were also used to calculate an intensity-weighted center of mass of the vimentin network (CM_{vim}) weighting the coordinates of each pixel within the cell spreading area by its green channel intensity. ΔCM was calculated as $|CM_{cell} - CM_{vim}|$. These last calculations were performed using a home-made Python routine.

2.8. Lateral motion of intermediate filaments

The lateral position of a filament segment was computed as its mean y coordinate ($\bar{y}$). The mean lateral square displacement (MSD_L) was calculated as [34]:

$$MSD_L = \langle(\bar{y}(t) - \bar{y}(t+\tau))^2\rangle \quad (4)$$

where t and τ are the absolute and lag times, respectively, and the brackets represents the time average. This calculation was done for $\tau < 50\%$ of the total time of the trajectory.

The number of trajectories analyzed for the live-cells experiments and fixed-cells measurements was 43 and 27, respectively.

2.9. Numerical simulations

To simulate filaments with shapes following a thermal distribution, we sampled the mode amplitudes a_n from a normal distribution with variances given by Eq. 6, a persistence length of 3 µm and $1 < n < 100$. The filaments lengths L were sampled from a uniform distribution in the range 0.5–6 µm. The number of simulated filaments was 250.

For each set of a_n, we computed θ(s) from Eq. (3) using 1 nm steps

for s and recovered the coordinates x and y along the filament as [45]:

$$x(\theta(s)) = \int_0^s \cos(\theta(s'))ds'$$

$$y(\theta(s)) = \int_0^s \sin(\theta(s'))ds' \quad (5)$$

Then, the filament shapes were re-sampled using a pixel size of 90 nm, *i.e.* similar to the experimental pixel size. When indicated, we added noise sampled from a normal distribution with a standard deviation of 20 nm to the y-coordinate.

2.10. Statistical analyses

Experimental results are expressed as mean ± standard error of the mean. Statistical significance among groups was analyzed using Welch two-sample *t*-test. Differences were considered significant for $p < .05$ and labeled with an asterisk.

We used a linear regression procedure for adjusting Eq. (7) to the Fourier data; the standard error (SE) of lp* was obtained from the intercept's error propagation. The lp* values were considered different if their lp* ± SE intervals did not overlap. Differences between lp* values were labeled with the symbol #.

3. Results and discussion

3.1. Fourier analysis of vimentin IFs curvatures in living cells

The persistence length of filaments (lp) can be obtained by analyzing the shapes of the filaments through a Fourier decomposition procedure [43]. Specifically, in thermal equilibrium, the variance of the Fourier mode amplitudes averaged over uncorrelated filaments shapes ($Var(a_q)$) is related to the mode q_n (q in Eq. (6)) as [43]:

$$\ln(Var(a_q)) = -\ln(lp) - 2\ln q \quad (6)$$

On the other hand, it was demonstrated that microtubule curvatures in living cells followed a thermal-like distribution [34,43] characterized by:

$$\ln(Var(a_q)) = -\ln(lp^*) - 2\ln q \quad (7)$$

The apparent persistence length (lp*) of microtubules was significantly smaller than the *in vitro* lp showing that non-thermal, random forces act on these filaments in cells [33].Thus, these previous works show that the curvature analysis could provide clues on forces acting on filaments in living cells.

Based on these previous reports, we followed a similar approach to study vimentin IFs in living cells. Fig. 1A shows a representative, confocal image of a BHK cell expressing GFP-vimentin. The filaments form an intricate network of highly curved and overlapping filaments. In some regions, it is also possible to observe thick fibers or bundles previously described in the literature [46] and probably formed by a relatively large number of filaments.

In the experiments showed in the following sections, we focused the analyses in mesh-like regions of the network, selected vimentin filaments with relatively low fluorescence intensities and used the filament tracking routine AFTER [34] to recover the coordinates of segments of these IFs. Despite the optical resolution of confocal microscopy does not allow assuring that these structures correspond to single filaments, their relatively low intensity in comparison to other vimentin structures observed in the field suggests that they are probably formed by one or a relatively low number of filaments. Additionally, we did not analyze the fibrous structures mentioned above [46].

The intricate geometry of the IF network imposes a limit to the lengths of filament segments that can be tracked. Therefore, we first adapted the Fourier method used for the curvature analysis of equally-sized microtubule segments [34] to this complex scenario; Fig. 1B shows a simplified scheme of this new procedure. Specifically, the filament segments tracked with AFTER were sorted according to their lengths and the data set was split into M groups using a bin size of 500 nm. Those groups containing a low number of filaments (< 8) were discarded from further analyses and the remaining groups were treated as independent ensembles through Fourier decomposition assigning to each group a filament length equal to the bin center. Then, the whole data set was globally analyzed.

To test the performance of this analytical procedure, we simulated the shapes of thermally-equilibrated filaments with lp = 3 μm (*i.e.* similar to the *in vitro* lp of IFs) and L values in the range of those of IF segments experimentally tracked. We analyzed these shapes as described before and found that the simulated data followed the behavior expected from Eq. 6 with lp = 2.9 ± 0.1 μm (Fig. 1B) validating the procedure.

The error in the filament localization introduces deviations from the linearity at high frequencies [34,43]. Thus, we quantified the precision on the localization of IFs in fixed BHK cells expressing GFP-vimentin obtaining a value of ~20 nm (Supplemental Fig. 1). We explored how this tracking error affects the lp determination adding a white noise with an amplitude of 20 nm to the y-coordinates of the simulated filaments and analyzed the data as described before. Fig. 1C shows that the simulated data deviated as expected from the linear behavior thus, we only considered data with wave vectors > 5.5 μm^{-1} for the studies performed with BHK cells described in the following sections.

3.2. Vimentin IFs curvatures follow a pseudo-thermal behavior in living cells

We acquired confocal images of live BHK cells expressing GFP-vimentin and localized filament segments using AFTER. Fig. 2A shows the Fourier decomposition of IF curvatures analyzed with the procedure described in the previous section. The data followed the behavior expected according to Eq. 7 indicating a thermal-like distribution of vimentin IFs curvatures in living cells. The apparent persistence length obtained from these analyses was 2.2 ± 0.1 μm.

To assay if the ~200 nm lateral resolution achieved with confocal imaging [47] hide details of IFs curvatures that may affect the analysis, we examined confocal and stimulated emission depletion (STED) microscopy images acquired in identical regions of transformed and metastasizing BJ fibroblasts (BJF) with fluorescently-labeled vimentin filaments (Fig. 2B). The comparison of these images shows that the dimmer filamentous structures observed with confocal imaging normally correspond to single filaments according to STED images. We recovered the coordinates of the same set of filaments in both images and performed the Fourier analysis as described before.

Fig. 2C shows that these techniques provided identical information on the filaments curvatures. In both cases, the distribution followed a pseudo-thermal behavior and the lp* values were not significantly different.

In contrast to microtubules that present an apparent persistence length ~ 2 orders smaller than that observed *in vitro* [33,34], the lp* of vimentin IFs in BHK cells was very similar to that determined in solution (~2.1 μm, [48]) suggesting that the curvatures of these filaments are not affected by the intracellular milieu.

This statement is in apparent contradiction with a wealth of evidence demonstrating interactions of IFs with other cytoskeleton networks [32]. Moreover, intra and extracellular forces continuously remodel these networks and may also impact on IF curvatures.

Therefore, we next explored how IFs respond to mechanical perturbations caused by specific alterations of either the microtubule or the actin networks.

3.3. The cytoskeletal crosstalk modulates the apparent persistence length and lateral mobility of vimentin IFs

Microtubules in living cells experience large forces. For example, their polymerization against obstacles or barriers [49,50] produces a

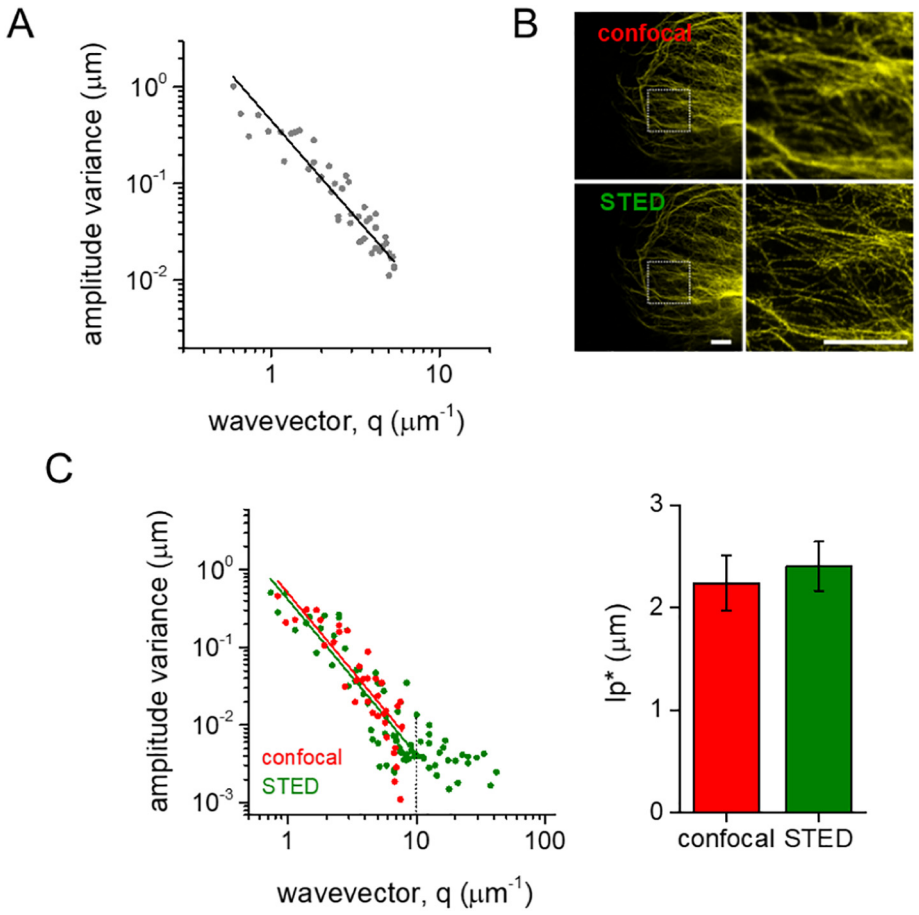

Fig. 2. Determination of the apparent persistence length of intermediate filaments in cells. (A) Fourier analysis of GFP-vimentin filaments tracked in live BHK cells ($N_{filaments}$ = 167, N_{cells} = 7). (B) Representative confocal and STED images obtained for BJF cells. Right panels show zoom-in regions (dotted squares in left images). Scale bars, 5 μm. (C) Fourier analyses of an identical set of filaments recovered from confocal and STED imaging of BJF cells. The higher spatial resolution of STED microscopy (30–50 nm) allows recovering the filaments position with higher precision thus; the data do not deviate from the linear behavior below the threshold indicated with a dotted line. ($N_{filaments}$ = 138, N_{cells} = 9).

pushing force that finally triggers their fast depolymerization [51] regulating the extension of the microtubule network. Therefore, we explored if those forces acting on microtubules also affect the IF network. With this aim, we incubated BHK cells with vinblastine that, at low concentrations, reduces the frequency of microtubule polymerization/depolymerization events [40].

Fig. 3A shows representative images of BHK cells expressing EMTB-3xGFP, protein that binds to microtubules. The images show that the accumulated tension in vinblastine-treated BHK cells increased the curvatures of microtubules in line with previous observations [52].

In contrast to the drastic alterations observed for microtubules, the overall morphology of the GFP-vimentin network in vinblastine-treated cells did not show major changes (Fig. 3A). We next explored if vinblastine affects the IF network in the mesh-like regions studying both, the lateral mobility of the filaments and their apparent persistence length.

We registered confocal time-stacks of regions of control and vinblastine-treated BHK cells expressing GFP-vimentin, tracked the lateral motion of IFs using AFTER and calculated the lateral mean squared displacement (MSD_L) from these trajectories as described in Materials and Methods. Fig. 3B shows that the suppression of microtubule dynamical stability significantly reduced the lateral mobility of vimentin filaments.

Fig. 3C and Supplemental Fig. 2 shows that vinblastine also increased ~65% the lp* of vimentin IFs. On the other hand, microtubules depolymerization at 4 °C with nocodazole did not affect lp* (Fig. 3C and Supplemental Fig. 3) suggesting that vimentin lp* is modulated by microtubules only when these last filaments are mechanically perturbed.

We showed before that the apparent persistence length of microtubules in living cells decreases after disrupting IFs indicating that the IF network restrains microtubule bucklings [34]. Relevantly, Fig. 3 suggests that mechanical forces acting on microtubules also affect the IF network.

Vimentin IFs link microtubules through several proteins such as APC [53], plectin [54] and the opposed-polarity microtubule motors kinesin and dynein [39,55,56] and indirectly through macromolecular complexes, organelles and other intracellular structures. In this context, we hypothesize that IFs linked directly or indirectly to microtubules in untreated cells are in a relaxed conformation with an lp* close to that measured *in vitro*. In contrast, when mechanical stresses are applied to microtubules, those IFs crosslinked to them straighten as a consequence of the tension causing an increase of their apparent persistence length and a reduction of their lateral mobility. In turn, the tension introduced in the associated IFs also limits the formation of more pronounced microtubule bucklings.

We next analyzed if perturbations in the actin network affect vimentin IFs properties in living cells. Vimentin IFs and actin contribute to cytoplasmic and cortical stiffness, respectively [6] and thus, both networks are intimately related with the cell response to external and internal forces. The biomechanical communication of these networks is fundamental in many processes including cell adhesion, migration and nuclear positioning [4,28–31].

We treated BHK cells expressing GFP-vimentin with latrunculin B (Lat−B), a well-known actin-depolymerizing drug. Relatively high concentrations of this drug caused the expected complete depolymerization of the actin network [57] with a concomitant collapse of the IF network into the perinuclear region (Supplemental Fig. 4). In contrast, a lower concentration of Lat-B did not modify drastically the cell shapes but reduced the cell spreading area and the number of stress fibers (Fig. 4A). Additionally, this treatment did not affect the relative distribution of the vimentin network as assessed by measuring the area

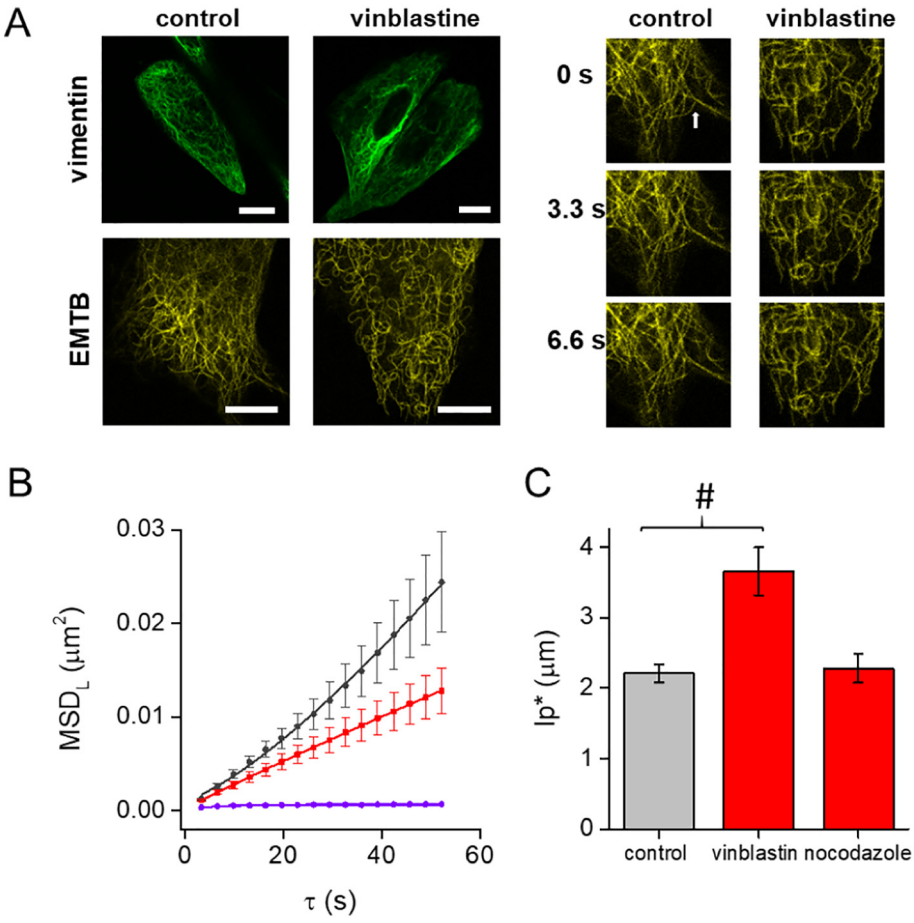

Fig. 3. Influence of the microtubule network in the apparent persistence length and lateral mobility of intermediate filaments. (A) Representative confocal images of BHK cells expressing GFP-vimentin or EMTB-GFP in control and vinblastine-treated conditions (left panels). Time-sequence registered in regions of cells expressing EMTB-GFP. The white arrow points to a microtubule catastrophe event. Microtubules in vinblastine-treated cells present increased curvatures. (right panels). (B) Lateral mean squared displacement of IFs determined in control (●), vinblastine-treated (●) and fixed (●) cells. (C) Apparent persistence lengths of vimentin IFs in control ($N_{filaments}$ = 167, N_{cells} = 7), vinblastin- ($N_{filaments}$ = 122, N_{cells} = 18) and nocodazole-treated cells ($N_{filaments}$ = 154, N_{cells} = 12). The symbol # indicates differences in lp* values, determined as described in Materials and Methods.

covered by the IF network relative to the cell spreading area (IF coverage) and the weighted center of mass of the IF network in comparison to the geometric cell center of mass (ΔCM, Supplemental Fig. 5). In agreement with our observations a similar mild Lat-B treatment in fibroblasts reduced the cell stiffness but did not produce visible modifications of the overall organization of the actin network [57].

We used AFTER to track IFs in Lat-B treated BHK cells expressing GFP-vimentin and verified that their lateral mobility significantly increased (Fig. 4B) suggesting that the treatment released IF filaments previously anchored to actin-related structures. It is worth mentioning that previous analysis of trajectories of organelles or particles in cells revealed that the behavior of the MSD plot may change with τ reflecting distinct motion regimes caused by forces acting in different temporal windows (see for example, [58–60]). Our relatively low frame acquisition frequency does not allow observing details of the MSD behavior for $\tau < 3.3$ s. Thus, the first point captured in the experiment seem to be an outlier of the behavior observed at longer τ but may reflect the presence of a different motion mechanism acting in a shorter time scale. For example, the thermal jittering of filaments may determine the shape of the MSD plot at low τ values whereas the observed behavior at longer τ probably includes the direct/indirect action of active forces such as those produced by molecular motors and/or polymerization/depolymerization of cytoskeleton components.

On the other hand, the Fourier analysis of IFs curvatures in living cells after the milder Lat-B treatment shows that the curvatures followed a thermal-like behavior (Supplemental Fig. 6). The lp* value was ~ 20% higher than that determined in control cells (Fig. 4C). This result is surprising since the reduction of the spreading area of the cells suggest that compressive forces may compact the IF network and thus increase the curvature of filaments.

In vitro assays show that IFs electrostatically interact producing thicker, self-associated bundles [61]. Additionally, we mentioned above previous works suggesting that IFs can self-associate in cells forming fibers or bundles that coalign with the orientation of traction stresses [46]. We then hypothesize that the partial depolymerization of the actin network may release vimentin filaments previously anchored to actin-related structures and allow their self-association forming relatively more rigid structures and thus resulting in a higher apparent persistence length. The persistence length of a filament is proportional to its flexural rigidity, which in turn depends on the elastic properties of the material and the filament geometry. Particularly, lp = EI/kT [18] where E is the Young's modulus and I is the second moment of inertia of the cross-section, which is proportional to the fourth-power of the filament radius for an isotropic and homogeneous cylindrical filament. Assuming that the intrinsic mechanical properties of the filament are conserved, this relation predicts that the increase on lp* observed after Lat-B treatment involves a ~ 5% increment on the effective radius of the filaments. This slight variation suggests that only a small fraction of the vimentin IFs filaments in mesh-like regions self-associates forming thicker and stiffer bundles after Lat-B treatment. We should emphasize that these subtle changes in the network could not be observed by standard imaging but are indirectly detected through the filaments curvature analysis.

The IF self-association process could compensate the partial loss of the stiffer actin filaments limiting abrupt changes of cell shape. Relevantly, Janmey et al. [24] proposed that the vimentin network might prevent cell deformation in the presence of perturbations that rupture actin network.

Taken together, these results show that both, microtubule and actin networks, modulate the apparent persistence length and lateral mobility of IFs in living cells.

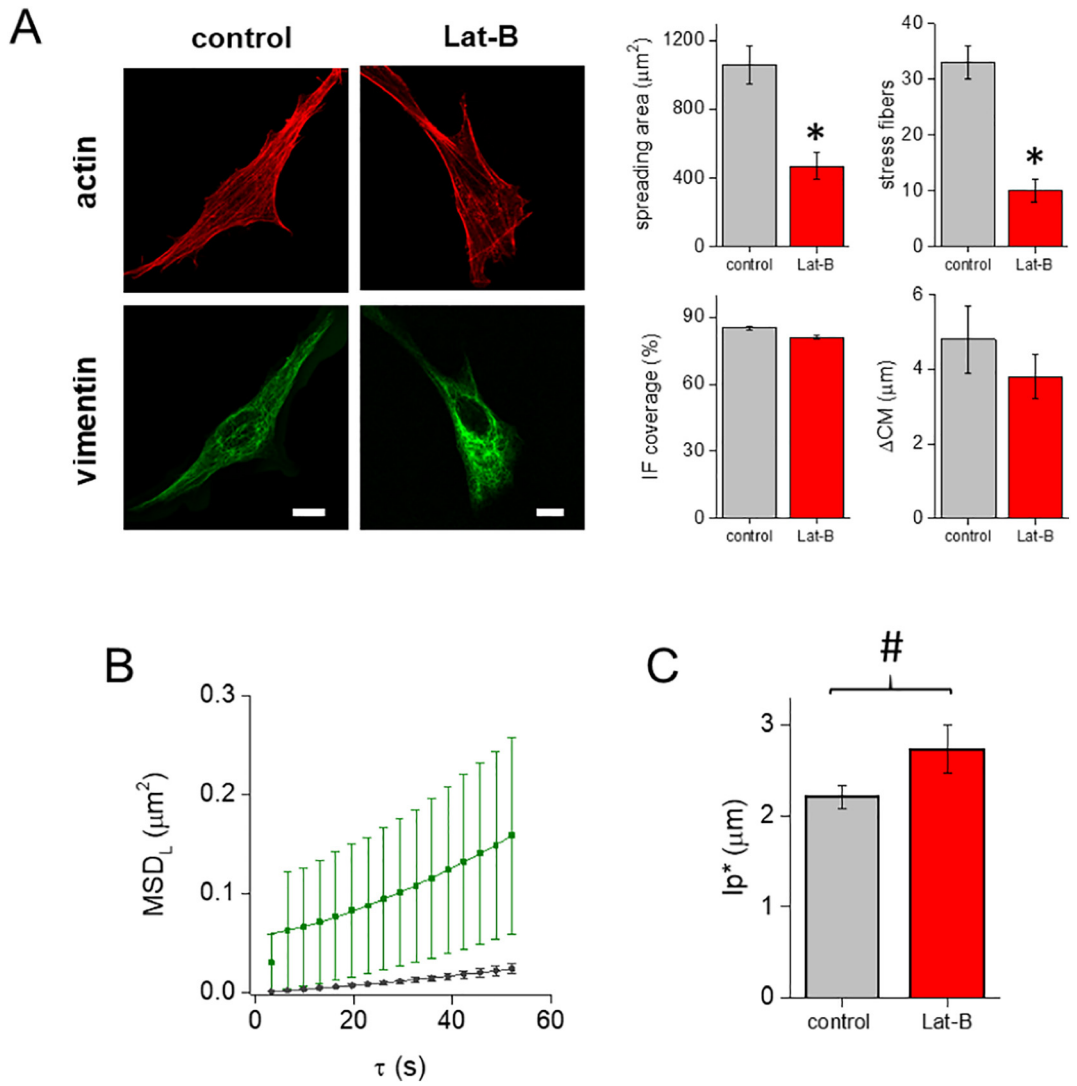

Fig. 4. Influence of the actin network in the lateral mobility and apparent persistence length of intermediate filaments. (A) Representative confocal images of fixed control or Lat-B treated BHK cells expressing GFP-vimentin and labeled with phalloidin Texas Red-X. The bar plots compiled the effects of the milder Lat-B treatment on certain morphological properties (N_{cells} = 31 and 35 for control and Lat-B conditions, respectively). (B) Lateral mean squared displacement of IFs determined in control (◆) and Lat-B treated (■) live cells ($N_{trajectories}$ = 43 in each condition). (C) Apparent persistence length of vimentin IFs in in control ($N_{filaments}$ = 167, N_{cells} = 7) and Lat-B treated live cells ($N_{filaments}$ = 149, N_{cells} = 24). The symbol # indicates differences in lp* values, determined as described in Materials and Methods.

4. Conclusions

The application of rheological methods to reconstituted IF networks provides many clues regarding the unusual mechanical properties of intermediate filaments [17,19]. However, the complex cellular environment defines that many properties of the IF network in living cells are not simply extrapolations of those observed *in vitro*.

Here, we used a filament localization routine to track vimentin IFs in living cells with nanometer precision and determined their apparent persistence length and lateral mobility. These properties provided relevant information on the mechanical properties of the filaments in their natural environment.

Interestingly, the curvatures of vimentin IFs in BHK cells followed a thermal-like behavior with an lp* value of 2.2 μm, slightly higher than the persistence length of these filaments deposited in substrates (0.3–1 μm, [62]) and similar to that measured in aqueous solution (2.1 μm, [48]). Importantly, it was reported that the interactions IF-substrate affect the curvatures and thus the lp of these filaments [62].

We mentioned before previous works showing that microtubules curvatures in cells also follow a thermal-like distribution but with apparent persistence length ~ 2 orders smaller than that expected from *in vitro* determinations [33,34]. These observations were explained considering that non-thermal, random forces increase the curvatures of microtubules in cells [33,34]. In this context, the similarity of the apparent persistence length of vimentin IFs in cells with that measured in aqueous solution suggests that vimentin filaments do not experience large forces in the intracellular environment. This asseveration does not imply that IFs are a passive component of the cytoskeleton. In fact, we verified that mechanical stresses introduced through the actin or microtubule networks modulate the vimentin IFs curvature distribution and their lateral mobility.

Specifically, the inhibition of microtubule dynamic instability increased the lp* of vimentin IFs and reduced their lateral mobility indicating that forces acting on microtubules also affect IFs. It has been proposed that the vimentin network act as a template for microtubules growing, constituting a mechanism to preserve cell polarity during migration [63]. We speculate that, in contrast to a passive template, vimentin filaments respond mechanically to forces acting on microtubules. Consequently, IFs provide a stiffer environment to microtubules experiencing high loads in living cells allowing them to hold

against these forces without buckling.

We have also observed that vimentin lp* depends on the actin network integrity. Specifically, vimentin lp* increased after partial depolymerization of actin possibly due to a higher proportion of self-associated and stiffer IF structures that may help to prevent the loss of the cell shape.

Recently, Costigliola et al. [46] analyzed morphologically the IF network in fibroblasts, observed fibers that aligned in the migration direction and proposed that they are required for the orientation of the traction stresses. In this work, we also detected that lp* and the lateral mobility of filaments in mesh-like regions of the IFs network are also affected when cells are mechanically perturbed. These observations suggest that subtler but mechanically relevant changes in the IF network occur under stress, in addition to the formation of thick fibers.

Taken together, our results evidence the mechanical coupling of vimentin IFs with the microtubule and the actin networks in living cells and contribute to understand the role of IFs network in mechanically stressed situations.

CRediT authorship contribution statement

Mariano Smoler:Conceptualization, Formal analysis, Investigation, Writing - original draft, Writing - review & editing, Visualization.**Giovanna Coceano**:Formal analysis, Investigation, Visualization, Writing - original draft.**Ilaria Testa**:Conceptualization, Methodology, Software, Formal analysis, Writing - original draft, Writing - review & editing.**Luciana Bruno**:Conceptualization, Methodology, Formal analysis, Writing - original draft, Writing - review & editing.**Valeria Levi**:Visualization, Supervision, Project administration.

Acknowledgements

This work was supported by ANPCyT [grant numbers PICT 2015-0370 and PICT-2016-0828]; UBACyT [grant number 20020150100122BA]; and CONICET [grant number PIP 11220130100121CO].

Declaration of competing interest

The authors declare that they have no known competing financial interests or personal relationships that could have appeared to influence the work reported in this paper.

Appendix A. Supplementary data

Supplementary data to this article can be found online at https://doi.org/10.1016/j.bbamcr.2020.118726.

References

[1] D. Mizuno, C. Tardin, C.F. Schmidt, F.C. Mackintosh, Nonequilibrium mechanics of active cytoskeletal networks, Science 315 (2007) 370–373.
[2] A.F. Pegoraro, P. Janmey, D.A. Weitz, Mechanical Properties of the Cytoskeleton and Cells, Cold Spring Harbor Perspectives in Biology, 9, (2017).
[3] D.A. Fletcher, R.D. Mullins, Cell mechanics and the cytoskeleton, Nature 463 (2010) 485–492.
[4] M.G. Mendez, S. Kojima, R.D. Goldman, Vimentin induces changes in cell shape, motility, and adhesion during the epithelial to mesenchymal transition, FASEB journal: official publication of the Federation of American Societies for Experimental Biology 24 (2010) 1838–1851.
[5] M.G. Mendez, D. Restle, P.A. Janmey, Vimentin enhances cell elastic behavior and protects against compressive stress, Biophys. J. 107 (2014) 314–323.
[6] M. Guo, A.J. Ehrlicher, S. Mahammad, H. Fabich, M.H. Jensen, J.R. Moore, J.J. Fredberg, R.D. Goldman, D.A. Weitz, The role of vimentin intermediate filaments in cortical and cytoplasmic mechanics, Biophys. J. 105 (2013) 1562–1568.
[7] M.C. De Rossi, L. Bruno, A. Wolosiuk, M.A. Desposito, V. Levi, When size does matter: organelle size influences the properties of transport mediated by molecular motors, Biochim. Biophys. Acta 1830 (2013) 5095–5103.
[8] O.E. Nekrasova, M.G. Mendez, I.S. Chernoivanenko, P.A. Tyurin-Kuzmin, E.R. Kuczmarski, V.I. Gelfand, R.D. Goldman, A.A. Minin, Vimentin intermediate filaments modulate the motility of mitochondria, Mol. Biol. Cell 22 (2011) 2282–2289.
[9] B.M. Chung, J.D. Rotty, P.A. Coulombe, Networking galore: intermediate filaments and cell migration, Curr. Opin. Cell Biol. 25 (2013) 600–612.
[10] C. Leduc, S. Etienne-Manneville, Intermediate filaments in cell migration and invasion: the unusual suspects, Curr. Opin. Cell Biol. 32 (2015) 102–112.
[11] C. De Pascalis, C. Perez-Gonzalez, S. Seetharaman, B. Boeda, B. Vianay, M. Burute, C. Leduc, N. Borghi, X. Trepat, S. Etienne-Manneville, Intermediate filaments control collective migration by restricting traction forces and sustaining cell-cell contacts, J. Cell Biol. 217 (2018) 3031–3044.
[12] R. Sanghvi-Shah, G.F. Weber, Intermediate filaments at the junction of Mechanotransduction, migration, and development, Frontiers in Cell and Developmental Biology 5 (2017) 81.
[13] S. Osmanagic-Myers, T. Dechat, R. Foisner, Lamins at the crossroads of mechanosignaling, Genes Dev. 29 (2015) 225–237.
[14] S.V. Strelkov, H. Herrmann, U. Aebi, Molecular architecture of intermediate filaments, Bioessays 25 (2003) 243–251.
[15] S. Etienne-Manneville, Cytoplasmic intermediate filaments in cell biology, Annu. Rev. Cell Dev. Biol. 34 (2018) 1–28.
[16] S. Koster, D.A. Weitz, R.D. Goldman, U. Aebi, H. Herrmann, Intermediate filament mechanics in vitro and in the cell: from coiled coils to filaments, fibers and networks, Curr. Opin. Cell Biol. 32 (2015) 82–91.
[17] E.E. Charrier, P.A. Janmey, Mechanical properties of intermediate filament proteins, Methods Enzymol. 568 (2016) 35–57.
[18] J. Howard, Mechanics of Motor Proteins and the Cytoskeleton, Sinauer Associates, Sunderland, MA, 2001.
[19] J. Block, V. Schroeder, P. Pawelzyk, N. Willenbacher, S. Koster, Physical properties of cytoplasmic intermediate filaments, Biochim. Biophys. Acta 1853 (2015) 3053–3064.
[20] T. Yanagida, M. Nakase, K. Nishiyama, F. Oosawa, Direct observation of motion of single F-actin filaments in the presence of myosin, Nature 307 (1984) 58–60.
[21] B. Mickey, Rigidity of microtubules is increased by stabilizing agents, J. Cell Biol. 130 (1995) 909–917.
[22] R.A. Battaglia, S. Delic, H. Herrmann, N.T. Snider, Vimentin on the move: new developments in cell migration, F1000Research, 7 (2018).
[23] A.E. Patteson, A. Vahabikashi, K. Pogoda, S.A. Adam, K. Mandal, M. Kittisopikul, S. Sivagurunathan, A. Goldman, R.D. Goldman, P.A. Janmey, Vimentin protects cells against nuclear rupture and DNA damage during migration, J. Cell Biol. 218 (2019) 4079–4092.
[24] P.A. Janmey, U. Euteneuer, P. Traub, M. Schliwa, Viscoelastic properties of vimentin compared with other filamentous biopolymer networks, J. Cell Biol. 113 (1991) 155–160.
[25] Y.C. Lin, N.Y. Yao, C.P. Broedersz, H. Herrmann, F.C. Mackintosh, D.A. Weitz, Origins of elasticity in intermediate filament networks, Phys. Rev. Lett. 104 (2010) 058101.
[26] P.A. Janmey, D.R. Slochower, Y.H. Wang, Q. Wen, A. Cebers, Polyelectrolyte properties of filamentous biopolymers and their consequences in biological fluids, Soft Matter 10 (2014) 1439–1449.
[27] Y.C. Lin, C.P. Broedersz, A.C. Rowat, T. Wedig, H. Herrmann, F.C. Mackintosh, D.A. Weitz, Divalent cations crosslink vimentin intermediate filament tail domains to regulate network mechanics, J. Mol. Biol. 399 (2010) 637–644.
[28] B.T. Helfand, M.G. Mendez, S.N. Murthy, D.K. Shumaker, B. Grin, S. Mahammad, U. Aebi, T. Wedig, Y.I. Wu, K.M. Hahn, M. Inagaki, H. Herrmann, R.D. Goldman, Vimentin organization modulates the formation of lamellipodia, Mol. Biol. Cell 22 (2011) 1274–1289.
[29] Y. Jiu, J. Peranen, N. Schaible, F. Cheng, J.E. Eriksson, R. Krishnan, P. Lappalainen, Vimentin intermediate filaments control actin stress fiber assembly through GEF-H1 and RhoA, J. Cell Sci. 130 (2017) 892–902.
[30] I. Dupin, Y. Sakamoto, S. Etienne-Manneville, Cytoplasmic intermediate filaments mediate actin-driven positioning of the nucleus, J. Cell Sci. 124 (2011) 865–872.
[31] Y. Jiu, J. Lehtimaki, S. Tojkander, F. Cheng, H. Jaalinoja, X. Liu, M. Varjosalo, J.E. Eriksson, P. Lappalainen, Bidirectional interplay between Vimentin intermediate filaments and contractile actin stress fibers, Cell Rep. 11 (2015) 1511–1518.
[32] F. Huber, A. Boire, M.P. Lopez, G.H. Koenderink, Cytoskeletal crosstalk: when three different personalities team up, Curr. Opin. Cell Biol. 32 (2015) 39–47.
[33] C.P. Brangwynne, F.C. MacKintosh, D.A. Weitz, Force fluctuations and polymerization dynamics of intracellular microtubules, Proc. Natl. Acad. Sci. U. S. A. 104 (2007) 16128–16133.
[34] C. Pallavicini, V. Levi, D.E. Wetzler, J.F. Angiolini, L. Bensenor, M.A. Desposito, L. Bruno, Lateral motion and bending of microtubules studied with a new single-filament tracking routine in living cells, Biophys. J. 106 (2014) 2625–2635.
[35] K. Faire, C.M. Waterman-Storer, D. Gruber, D. Masson, E.D. Salmon, J.C. Bulinski, E-MAP-115 (ensconsin) associates dynamically with microtubules in vivo and is not a physiological modulator of microtubule dynamics, J. Cell Sci. 112 (Pt 23) (1999) 4243–4255.
[36] W.C. Hahn, C.M. Counter, A.S. Lundberg, R.L. Beijersbergen, M.W. Brooks, R.A. Weinberg, Creation of human tumour cells with defined genetic elements, Nature 400 (1999) 464–468.
[37] M. Ratz, I. Testa, S.W. Hell, S. Jakobs, CRISPR/Cas9-mediated endogenous protein tagging for RESOLFT super-resolution microscopy of living human cells, Scientific Reports, 5 (2015).
[38] V. Levi, V.I. Gelfand, A.S. Serpinskaya, E. Gratton, Melanosomes transported by myosin-V in Xenopus melanophores perform slow 35 nm steps, Biophys. J. 90 (2006) L7–L9.

[39] C. Hookway, L. Ding, M.W. Davidson, J.Z. Rappoport, G. Danuser, V.I. Gelfand, Microtubule-dependent transport and dynamics of vimentin intermediate filaments, Mol. Biol. Cell 26 (2015) 1675–1686.
[40] A. Robert, H. Herrmann, M.W. Davidson, V.I. Gelfand, Microtubule-dependent transport of vimentin filament precursors is regulated by actin and by the concerted action of Rho- and p21-activated kinases, FASEB journal: official publication of the Federation of American Societies for Experimental Biology 28 (2014) 2879–2890.
[41] P.D. Wasserman, Advanced Methods in Neural Computing, Van Nostrand Reinhold, New York, 1993.
[42] S. Haykin, Neural Networks: A Comprehensive Foundation 2nd. ed., Prentice hall, Upper Saddle River, New Jersey, 1999.
[43] F. Gittes, B. Mickey, J. Nettleton, J. Howard, Flexural rigidity of microtubules and actin filaments measured from thermal fluctuations in shape, J. Cell Biol. 120 (1993) 923–934.
[44] J. Schindelin, I. Arganda-Carreras, E. Frise, V. Kaynig, M. Longair, T. Pietzsch, S. Preibisch, C. Rueden, S. Saalfeld, B. Schmid, J.Y. Tinevez, D.J. White, V. Hartenstein, K. Eliceiri, P. Tomancak, A. Cardona, Fiji: an open-source platform for biological-image analysis, Nat. Methods 9 (2012) 676–682.
[45] F. Gittes, E. Meyhofer, S. Baek, J. Howard, Directional loading of the kinesin motor molecule as it buckles a microtubule, Biophys. J. 70 (1996) 418–429.
[46] N. Costigliola, L. Ding, C.J. Burckhardt, S.J. Han, E. Gutierrez, A. Mota, A. Groisman, T.J. Mitchison, G. Danuser, Vimentin fibers orient traction stress, Proc. Natl. Acad. Sci. U. S. A. 114 (2017) 5195–5200.
[47] R. Rigler, U. Mets, J. Widengren, P. Kask, Fluorescence correlation spectroscopy with high count rate and low background: analysis of translational diffusion, Eur. Biophys. J. 22 (1993) 169–175.
[48] B. Noding, S. Koster, Intermediate filaments in small configuration spaces, Phys. Rev. Lett. 108 (2012) 088101.
[49] A.D. Bicek, E. Tuzel, A. Demtchouk, M. Uppalapati, W.O. Hancock, D.M. Kroll, D.J. Odde, Anterograde microtubule transport drives microtubule bending in LLC-PK1 epithelial cells, Mol. Biol. Cell 20 (2009) 2943–2953.
[50] I.A. Kent, P.S. Rane, R.B. Dickinson, A.J. Ladd, T.P. Lele, Transient pinning and pulling: a mechanism for bending microtubules, PLoS One 11 (2016) e0151322.
[51] M.E. Janson, M.E. de Dood, M. Dogterom, Dynamic instability of microtubules is regulated by force, J. Cell Biol. 161 (2003) 1029–1034.
[52] R. Dhamodharan, M.A. Jordan, D. Thrower, L. Wilson, P. Wadsworth, Vinblastine suppresses dynamics of individual microtubules in living interphase cells, Mol. Biol. Cell 6 (1995) 1215–1229.
[53] Y. Sakamoto, B. Boeda, S. Etienne-Manneville, APC binds intermediate filaments and is required for their reorganization during cell migration, J. Cell Biol. 200 (2013) 249–258.
[54] G. Wiche, S. Osmanagic-Myers, M.J. Castanon, Networking and anchoring through plectin: a key to IF functionality and mechanotransduction, Curr. Opin. Cell Biol. 32 (2015) 21–29.
[55] C. Leduc, S. Etienne-Manneville, Regulation of microtubule-associated motors drives intermediate filament network polarization, J. Cell Biol. 216 (2017) 1689–1703.
[56] V. Prahlad, M. Yoon, R.D. Moir, R.D. Vale, R.D. Goldman, Rapid movements of vimentin on microtubule tracks: kinesin-dependent assembly of intermediate filament networks, J. Cell Biol. 143 (1998) 159–170.
[57] T. Wakatsuki, B. Schwab, N.C. Thompson, E.L. Elson, Effects of cytochalasin D and latrunculin B on mechanical properties of cells, J. Cell Sci. 114 (2001) 1025–1036.
[58] L. Bruno, V. Levi, M. Brunstein, M.A. Desposito, Transition to superdiffusive behavior in intracellular actin-based transport mediated by molecular motors, Phys. Rev. E Stat. Nonlinear Soft Matter Phys. 80 (2009) 011912.
[59] M. Brunstein, L. Bruno, M. Desposito, V. Levi, Anomalous dynamics of melanosomes driven by myosin-V in Xenopus laevis melanophores, Biophys. J. 97 (2009) 1548–1557.
[60] C. Metzner, C. Raupach, C.T. Mierke, B. Fabry, Fluctuations of cytoskeleton-bound microbeads–the effect of bead-receptor binding dynamics, J Phys Condens Matter 22 (2010) 194105.
[61] M. Schopferer, H. Bar, B. Hochstein, S. Sharma, N. Mucke, H. Herrmann, N. Willenbacher, Desmin and vimentin intermediate filament networks: their viscoelastic properties investigated by mechanical rheometry, J. Mol. Biol. 388 (2009) 133–143.
[62] N. Mucke, L. Kreplak, R. Kirmse, T. Wedig, H. Herrmann, U. Aebi, J. Langowski, Assessing the flexibility of intermediate filaments by atomic force microscopy, J. Mol. Biol. 335 (2004) 1241–1250.
[63] Z. Gan, L. Ding, C.J. Burckhardt, J. Lowery, A. Zaritsky, K. Sitterley, A. Mota, N. Costigliola, C.G. Starker, D.F. Voytas, J. Tytell, R.D. Goldman, G. Danuser, Vimentin intermediate filaments template microtubule networks to enhance persistence in cell polarity and directed migration, Cell Systems 3 (2016) 252–263 (e258).